Use of Acetylcholine Binding Protein in the Search for Novel α7 Nicotinic Receptor Ligands. In Silico Docking, Pharmacological Screening, and X-ray Analysis†

Chris Ulens,[¶,◆] Atilla Akdemir,[§,◆] Aldo Jongejan,[§] Rene van Elk,[‡] Sonia Bertrand,[▽] Anastassis Perrakis,[¶] Rob Leurs,[§] August B. Smit,[‡] Titia K. Sixma,[¶] Daniel Bertrand,[▽] and Iwan J. P. de Esch*[,§]

Division of Molecular Carcinogenesis, Netherlands Cancer Institute, Amsterdam, The Netherlands, Leiden/Amsterdam Center for Drug Research (LACDR), Division of Medicinal Chemistry, Faculty of Sciences, VU University Amsterdam, Amsterdam, The Netherlands, Department of Molecular and Cellular Neurobiology, Institute of Neurosciences, Faculty of Earth and Life Sciences, VU University Amsterdam, Amsterdam, The Netherlands, and Department of Neuroscience, Centre Medical Universitaire, Geneva, Switzerland

Received November 6, 2008

Acetylcholine binding protein (AChBP) is widely considered as a functional and structural homologue of the ligand binding domain of Cys-loop receptors. We report the use of AChBP as template to identify ligands for the nicotinic receptors (nAChRs). An in silico screening protocol was set up and applied to crystal structures of AChBP. Several ligands containing a dibenzosuberyl moiety were identified and shown to bind with high affinity to AChBP and α7 nAChRs. Two high affinity ligands were cocrystallized with AChBP, revealing the binding mode in the orthosteric site. Functional studies revealed that these two ligands caused inhibition of the α7, α4β2, and $5HT_3$ receptors. The noncompetive blockade of the receptors suggests that these compounds act by steric hindrance of the channel. The analysis of the dual binding mode of these dibenzosuberyl-containing compounds can lead to better understanding of the complex mode of action of similar tricyclic ligands on Cys-loop receptors.

Introduction

The nicotinic acetylcholine receptor (nAChR[a]) is the prototypical member of the Cys-loop receptor family of ligand-gated ion channels that also includes the glycine, γ-aminobutyric acid (GABA-A and GABA-C), and serotonin ($5\text{-}HT_3$) receptors.[1] The nAChR is considered a major drug target, since neuronal nAChR subtypes are associated with brain diseases with high occurrence in the Western world. The human α4β2 and α7 nAChRs are likely to be involved in the pathophysiology of Alzheimer's disease, schizophrenia, epilepsy, and anxiety.[1] In addition, the human α4β2 nAChR is involved in nicotine addiction and pain[1] whereas the human α7 nAChR might also be a pharmacological target in inflammation.[2] Several nicotinic receptor ligands are being investigated for clinical use.[3] The first successes were reported in 2006, when varenicline, a partial agonist on the α4β2 nAChR, was approved as a drug for smoking cessation.[4] In spite of this important progress, discovery of nAChR specific ligands remains a challenge where a better knowledge of the binding site will represent a decisive step forward.

Structure-based drug discovery procedures to identify novel and selective ligands cannot be performed directly on the available three-dimensional structures of nAChRs because no high-resolution crystal structures of eukaryote nAChRs exist. Detailed knowledge of the structural architecture of the binding pocket has become available after the identification and structure determination of a eukaryotic homologue of the nAChR extracellular domain, namely, the acetylcholine binding protein (AChBP).[5,6] AChBPs from different snail species have been identified, and ligand-bound cocrystal structures have been determined.[6−13] Very recently, the first crystal structure of a prokaryotic homologue of the nAChR from the bacterium *Erwinia chrysanthemi* was solved,[14] but ligands for this receptor are unknown.

The crystal structures of the AChBPs from three different snail species show a conserved architectural fold that has been recognized as a template to construct homology models for the ligand binding domains of mammalian neurotransmitter receptors.[6,10,11] Crucial information on ligand−receptor interactions has been obtained from agonist-bound structures of AChBP, i.e., carbamylcholine, nicotine, and epibatidine.[8,12] Similar cation−π interactions between a conserved tryptophan and a cationic center in nonpeptidic nicotinic receptor ligands are observed in these cocrystal structures. Recently, we and others have determined cocrystal structures of AChBP from *Aplysia californica* (Ac-AChBP) in complex with the competitive inhibitor α-conotoxins[7,11] from venomous cone snails and from *Lymnaea stagnalis* (Ls-AChBP) in complex with nonpeptidic nAChR agonists.[7,8,11,12] Knowledge of the chemical interactions between these ligands and the receptor binding site has given detailed insight into the molecular determinants required for subtype-selective ligand binding.[7,8,10,12]

We hypothesized that the rational discovery of new lead compounds with improved subtype selectivity for human nAChRs could be pursued by using crystal structures of AChBP as templates within in silico screening procedures. In the past, successful in silico screenings have been performed using crystal structures of various protein targets.[15−18] At the heart of these procedures are docking algorithms that aim to predict the optimal

† Coordinates of the protein in the apo state and in complex with compounds **31** and **35** have been deposited in the Protein Data Bank under accession codes 2w8e, 2w8f, and 2w8g, respectively.

* To whom correspondence should be addressed. Phone: +31-(0)20-5987841. Fax: +31-(0)20-5987610. E-mail: i.de.esch@few.vu.nl.

¶ Netherlands Cancer Institute.

◆ These authors have contributed equally.

§ Division of Medicinal Chemistry, VU University Amsterdam.

‡ Institute of Neurosciences, VU University Amsterdam.

▽ Centre Medical Universitaire.

[a] Abbreviations: AChBP, acetylcholine binding protein; nAChR, nicotinic acetylcholine receptor; SEM, standard error of the mean; ^{125}I-Bgt, [^{125}I]α-bungarotoxin; Ls-AChBP, acetylcholine binding protein from *Lymnaea stagnalis*; Ac-AChBP, acetylcholine binding protein from *Aplysia californica*; rmsd, root mean square deviation; FCS, fetal calf serum; GPCRs, G-protein-coupled receptors; PBS, phosphate buffered saline; BSA, bovine serum albumin; DMEM, Dulbecco's modified Eagle medium; PDB, Brookhaven Protein Data Bank; MLA, methyllycaconitine.

10.1021/jm801400g CCC: $40.75
Published on Web 03/30/2009

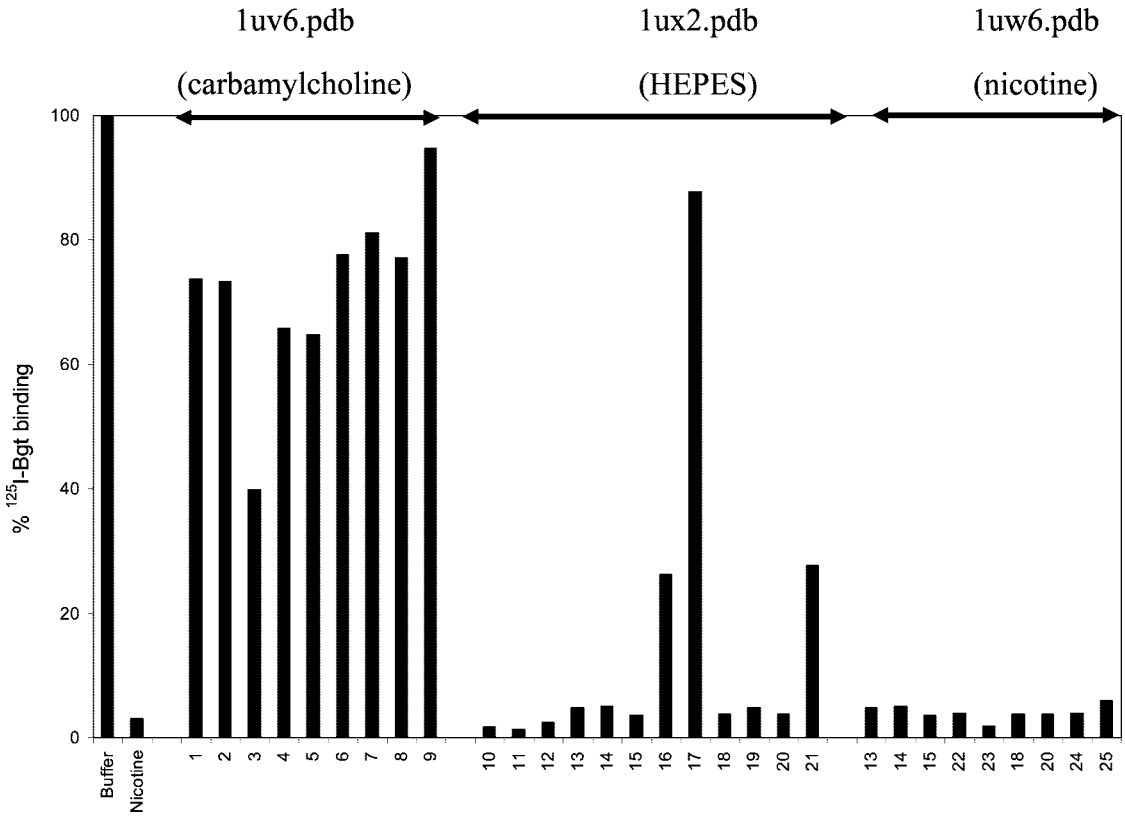

Figure 1. Single point ^{125}I-Bgt displacement from Ls-AChBP of the compounds (at 100 μM concentration) selected by in silico screening on the structures of carbamylcholine-AChBP, HEPES-AChBP, and nicotine-AChBP. The HEPES-AChBP and nicotine-AChBP structures were the most successful in the procedure. Note that five of the compounds identified with the HEPES-AChBP structure were also found with the nicotine-AChBP structure.

binding pose of ligands inside the binding pocket and their corresponding ligand−receptor interaction energy, i.e. tightness of binding. For this purpose, scoring functions are used to estimate ligand−receptor complementarity and the highest scoring binding poses generally show good intermolecular interaction of ligand and receptor.[19,20] Numerous combinations of docking algorithms and scoring functions have been explored in the literature.[15,16,19,20] In the present study, we applied the frequently used and thoroughly validated combination of the GOLD docking program and the GoldScore scoring function[21] using three different Ls-AChBP structures. The screening procedure was applied to a proprietary compound collection and consists of the actual docking, visual inspection for the binding pose, pharmacological assays, and an analogue search. Using this approach, we discovered novel classes of small molecule AChBP ligands, some of which also have good affinity for the human α7 nAChR. To gain insight into the interaction of these ligands and the receptor binding site, we cocrystallized two novel tricyclic hit compounds that were obtained from the in silico screen with AChBP. These structures provided novel insight in structure-based hit optimization and procedures to obtain subtype selective agonists for human nAChRs. Moreover, the results illustrate the use and limitations of the AChBP structure as a template in an in silico screening for novel nAChR ligands.

Results

In Silico Screening and Pharmacological Characterization. In order to discover novel ligands for human nAChRs, we carried out in silico screening studies using AChBP as template. Docking studies were performed using the three available crystal structures of Ls-AChBP, i.e., the AChBP complexes with carbamylcholine (PDB accession code 1uv6), HEPES (PDB accession code 1ux2), and nicotine (PDB accession code 1uw6).[12] Bound ligands and water molecules were removed from the AChBP models, whereafter in silico screening of an in-house compound collection containing druglike molecules was performed using the GOLD[21] docking program in combination with the GoldScore scoring function. The compounds were ranked according to their scores and the top-ranked 50 compounds were visually inspected for their binding pose. The top-ranked compounds with favorable binding poses, e.g. cation−π interactions, hydrogen bonding, and steric complementarity, were tested for [^{125}I]α-bungarotoxin (^{125}I-Bgt) displacement on Ls-AChBP using a single ligand concentration (100 μM) (Figure 1).

A first subset of nine compounds was identified from docking simulations using the carbamylcholine-AChBP structure. None of these compounds showed full ^{125}I-Bgt displacement (compounds **1**−**9**, Figure 1), even at a high concentration of 100 μM. Nevertheless, eight compounds display 20% or higher displacement of radioligand, including one compound with 60% radioligand displacement. A second subset of 12 compounds was selected in an in silico screen on the HEPES-AChBP structure. Nine of these 12 compounds displaced ^{125}I-Bgt to the same extent as nicotine (compounds **10** − **21**, Figure 1). The final in silico screen was performed on the nicotine-AChBP structure. The top-ranked list included five of the compounds already identified in the screen on the HEPES-AChBP structure (compounds **13**−**15**, **18**, **20**). Four additional compounds were selected for single point displacement assays, and all of them showed ^{125}I-Bgt displacement similar to nicotine (compounds **22** − **25**, Figure 1).

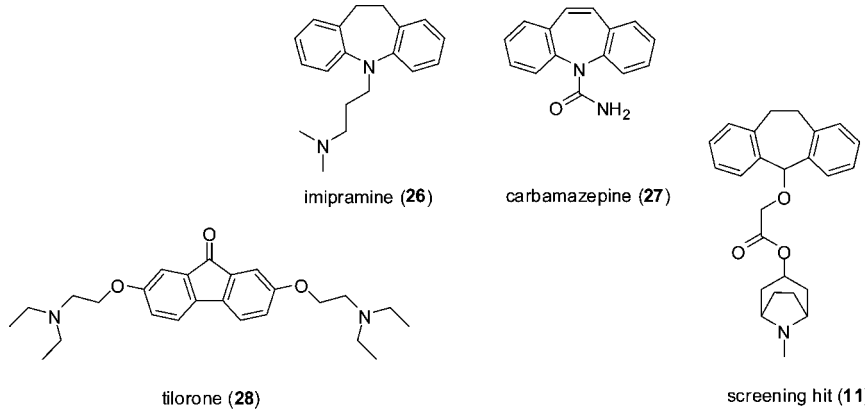

Figure 2. Structures of known tricyclic nAChR ligands.

In total, we selected 16 compounds using the HEPES and nicotine bound AChBP structures in the in silico screening, and we determined their binding affinity for Ls-AChBP. We identified 13 compounds with a similar affinity for Ls-AChBP as nicotine. In contrast, binding affinities for Ls-AChBP of a randomly selected set of compounds from our compound collection resulted in an 8-fold lower hit rate, validating the high enrichment obtained from the in silico screening protocol.

Inspection of the identified hit structures revealed a compound that contained a tricyclic (dibenzosuberyl) moiety (**11**, Figure 2). This moiety is reminiscent of the pharmacophore found in certain psychotropic drugs, such as the class of tricyclic antidepressants (e.g., imipramine, **26**, Figure 2). In early studies, these promiscuous drugs were suggested to bind to the ion channel pore of nAChRs.[22] Other known tricyclic nAChR ligands include the antiepileptic carbamazepine (**27**, Figure 2) and the tricyclic interferon inducer tilorone (**28**, Figure 2) that was very recently identified by Abbott researchers as a selective partial agonist for α7 nAChRs.[23]

Being intrigued by our tricyclic hit structure **11**, we searched our proprietary database for other dibenzosuberyl-containing derivatives. A total of 13 compounds were available, and ^{125}I-Bgt displacement assays on Ls-AChBP revealed that these ligands have affinities in the same range as those found for acetylcholine and nicotine (compounds **29**−**41**, pK_i values of 5.5−7.2, Tables 1 and 2, Figure 3). When taking compound **29** as a reference compound of this series, we showed that methylation of the tropine nitrogen atom does not have a significant effect on the Ls-AChBP affinity. However, increasing the substituent by a hydrophobic ethyl group or a benzyl moiety increases the binding affinity. More polar substituents that are attached to the tropine nitrogen atom lead to somewhat lower affinity compounds (**36**, **37**, **38**). Substitution of the R_3 position on the aromatic ring leads to a significant increase in affinity, whereas a similar small substituent in the R_4 position does not alter the binding to AChBP. Interestingly, tropine containing ligands have significantly higher affinity for Ls-AChBP than their piperidine analogues (Table 2; compare **39** with **29** and compare **40** with **30**). Compound **41** indicates that attachment of bigger hydrophobic substituents can increase the binding affinity, as was shown for the tropine derivatives.

The highest affinity was observed for compounds **31** and **35** (Table 1, Figure 3), and these were comparable to that of nicotine (**31** pK_i = 7.2 ± 0.1, **35** pK_i = 7.0 ± 0.1, nicotine pK_i = 7.2 ± 0.1, on Ls-AChBP). We note that both **31** and **35** as well as nicotine were not within the top-ranked compounds that were visually inspected. The structural identity of these compounds and their binding affinities for the target proteins were confirmed by resynthesis, chemical characterization of the synthesized molecules, and retesting.

Table 1. Binding Affinities (pK_i ± SEM) for Ls-AChBP of the in Silico Identified Compound **11** and Its Analogues

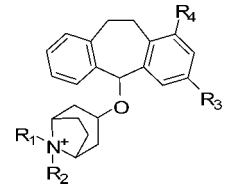

Number	R_1	R_2	R_3	R_4	pK_i ± SEM
29	H	H	H	H	6.5 ± 0.2
30	CH_3	H	H	H	6.4 ± 0.1
31	CH_3	CH_3	H	H	7.2 ± 0.1
32	CH_3	H	CH_3	H	6.9 ± 0.1
33	CH_3	H	H	CH_3	6.5 ± 0.4
34	CH_2CH_3	H	H	H	6.9 ± 0.1
35		H	H	H	7.0 ± 0.1
36		H	H	H	5.9 ± 0.2
37		H	H	H	6.3 ± 0.2
38		H	H	H	6.0 ± 0.2
Nicotine					7.2 ± 0.1
Acetylcholine					5.5 ± 0.1
11					7.0 ± 0.1

Subsequently, we tested these compounds in a ^{125}I-Bgt displacement assay on SH-SY5Y cells, which have previously been shown to express the human α7 nAChR.[24,25] Interestingly, **31** binds with affinity comparable to nicotine, whereas **35** has a lower affinity (**31** pK_i = 5.7 ± 0.2, **35** pK_i = 4.9 ± 0.1, nicotine pK_i = 6.0 ± 0.1, on human α7 nAChR). This illustrates small differences between the AChBP and α7 nAChR binding sites that are probed by this series of compounds. Finally, these two compounds were tested in an [^{3}H]epibatidine displacement assay on human α4β2 nAChRs (transiently transfected in HEK293t cells), and no binding was observed. This is in line with the similar pharmacological characteristics of Ls-AChBP and the human α7 nAChR.[5,6]

Cocrystal Structures of 31 and 35 with Ac-AChBP. To validate our in silico screening protocol and to gain insight into

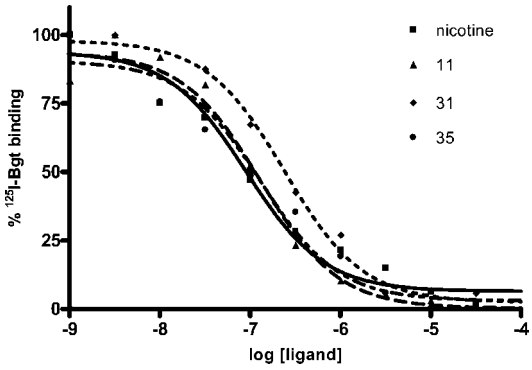

Figure 3. ^{125}I-Bgt displacement curves on Ls-AChBP are shown. Compound **11** (▲) was identified by in silico screening and has a similar affinity as nicotine (■). The chemical analogue search in our proprietary compound collection resulted in the identification of several compounds including **31** (◆) and **35** (●).

Table 2. Structure and Binding Affinity (pK_i ± SEM) of Piperidine Containing Analogues of the Tricyclic Compounds

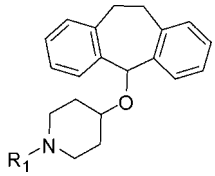

compd	R_1	pK_i ± SEM
39	H	5.5 ± 0.1
40	CH_3	5.8 ± 0.2
41	$CH_2CH_2CH_3$	6.2 ± 0.1

the structural recognition of these newly discovered compounds by the AChBP binding site, we solved cocrystal structures of AChBP with selected compounds obtained in our in silico screening. The dibenzosuberyl-containing analogues **31** and **35**, which have the highest affinity for Ls-AChBP and show selectivity for the human α7 nAChR, were selected as the best candidates for cocrystallization with AChBP. Because cocrystals of Ac-AChBP often have better diffraction quality than those obtained with Ls-AChBP, we cocrystallized **31** and **35** with Ac-AChBP. Both compounds were tested in [^{3}H]epibatidine displacement studies on Ac-AChBP, and their binding affinities were similar to the affinity of nicotine (**31** pK_i = 6.3 ± 0.2, **35** pK_i = 6.0 ± 0.2, nicotine pK_i = 6.4 ± 0.1, on Ac-AChBP).

The structure of Ac-AChBP in complex with **31** was solved by molecular replacement at 2.7 Å resolution. The model was refined to R_{work} = 23.7% and R_{free} = 26.7% with good geometry (Table 3). The structure of the **31**-bound complex is similar to other complexes of Ac-AChBP except that loop C, which wraps around the ligand-binding site, has a conformation that is intermediate between the fully contracted state observed in AChBP complexes with agonists and the extended state observed in complexes with antagonists such as α-conotoxins. In the complex of Ac-AChBP with **31**, the maximal outward displacement of loop C amounts to ∼4.8 Å, as measured between the Cys188 C_α atom in this complex and the HEPES-bound complex of Ac-AChBP (Figures 4A,B). In comparison, the distance between the Cys188 C_α atom in the α-conotoxin bound complex and the HEPES-bound complex is ∼11 Å. Loop C displays this intermediate conformation at all binding sites of the two pentamers present in the asymmetric unit. The binding orientation for **31** (Figure 4C) could only be resolved from difference electron density at two binding sites, which are also involved in a crystal contact between the two pentamers in the asymmetric unit. The remaining sites contain partial density for **31**, suggesting that part of the ligand may adopt multiple conformations in the binding pocket.

To provide additional experimental evidence for the binding mode of **31** in AChBP, we also solved the crystal structure of Ac-AChBP in complex with **35**, which crystallizes in a different crystal packing symmetry. The structure of this complex was determined at 2.8 Å resolution, and the model was refined to R_{work} = 20.0% and R_{free} = 25.0% with good geometry (Table 3). The asymmetric unit contains one pentamer, which has four binding sites characterized by an "intermediately" extended conformation of loop C, similar to the complex with **31**. The distance between the Cys188 C_α atom in the **35** bound complex and the HEPES-bound complex is 6.8 ± 0.4 Å.

Loop C of the fifth binding site is in the fully extended conformation because of its interaction with the extreme carboxy terminus of a neighboring pentamer in the crystal packing. This portion of the protein, Arg206−Asp217, was found to be disordered in all previous AChBP structures and was now for the first time built into electron density. The extreme C-terminus lacks secondary structure and extends along the surface of AChBP. The 12 amino acids that constitute the C-terminus are highly variable between different AChBPs and have no homology to the amino acid sequence that forms the interface with the transmembrane domain in nAChRs. It is therefore unlikely that knowledge of this structure adds to our understanding of receptor function.

Compound **35** could be fit automatically into difference electron density at two binding sites. The binding mode of **35** in these sites shows that the orientation of the molecule is similar to **31** except that the dibenzosuberyl moiety is rotated by ∼90° around the ether bond (Figure 4D). This observation supports the possibility that a certain degree of rotational or vibrational freedom of the tricyclic moiety around the ether bond exists and that this portion of the molecule might therefore be disordered in some binding sites. Partial density is observed in two binding sites of the **35** complex, indicating that the ligand adopts multiple conformations at these sites of the complex as well. The binding site involved in the crystal contact with the C-terminus of a neighboring pentamer reveals clear electron density for **35** but rotated by ∼160° with respect to the orientation observed in the other sites that do not interact with a C-terminal domain. At this particular site, **35** interacts with the side chains of Arg213 and Leu215 and the backbone of Asn214 of the C-terminal domain instead of the residues from the complementary binding site. Although not relevant to our understanding of the binding mode in nAChRs, this ligand orientation induced by the interaction with the nonconserved C-terminal domain from Ac-AChBP indicates that the binding mode is highly dependent on the chemical environment of the ligand.

We find that the binding orientations of **31** and **35** are different from the orientations predicted in the in silico screen. As illustrated in Figures 5A,B, our docking studies suggested two possible orientations of **31** within the contracted C-loop model of Ls-AChBP with the dibenzosuberyl moiety pointing either upward or downward in the binding cavity. Our crystal structures demonstrate that both **31** and **35** displace loop C outward by 5−6 Å, and as a result, the ligand occupies the binding pocket of Ac-AChBP in an orientation different from the one predicted in the in silico screen (parts C and E of Figure 5). In the orientation shown in parts C and E of Figure 5, **31** and **35** have their ethylene bridge of the tropine moiety pointing away from the aromatic residues of the principal face. At the

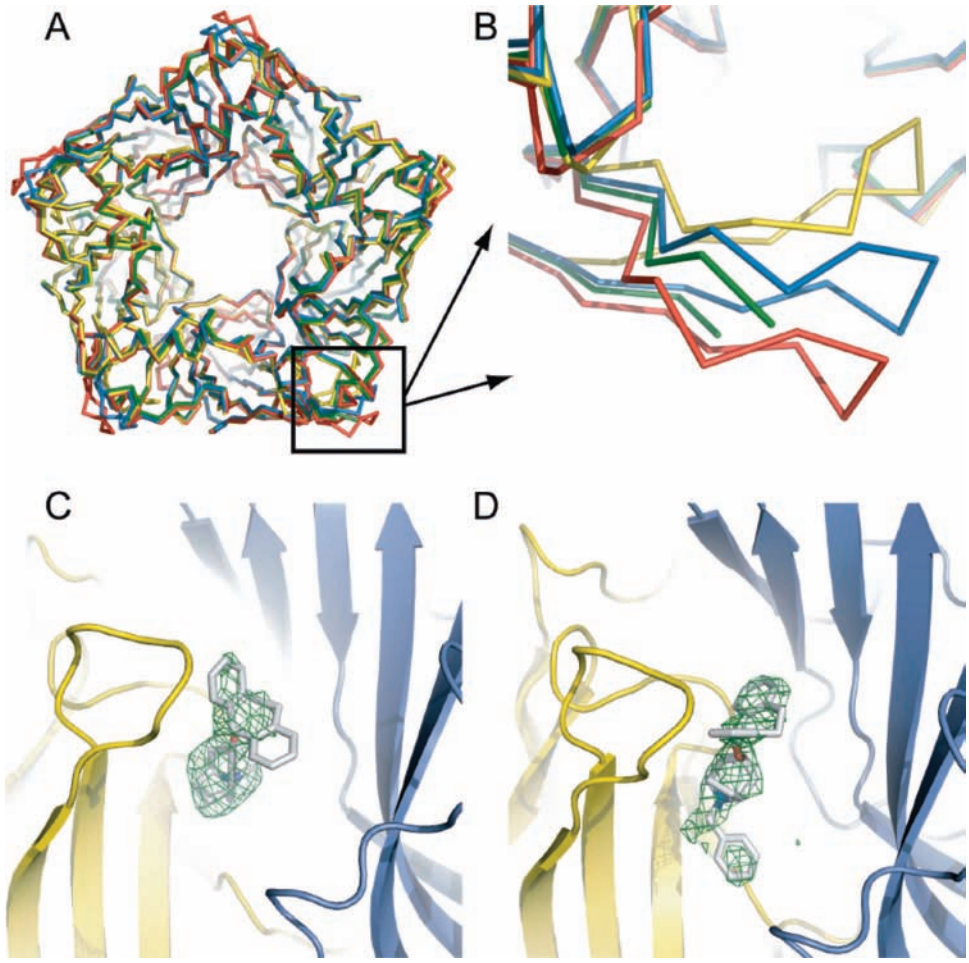

Figure 4. Ac-AChBP crystal structures in complex with HEPES (yellow), α-conotoxin (red), and **31** (blue) have been superposed (A) to illustrate the displacement of loop C upon ligand binding (B). Crystals of Ac-AChBP in the apo state (green) showed a lack of electron density for loop C, indicating that this region is flexible in the absence of ligand. **31** and **35** displace loop C (Cys188 C_α atoms) by ∼5 Å when compared to the HEPES-bound structure. The α-conotoxin-bound structure displaces loop C by ∼11 Å. The binding poses of **31** (C) and **35** (D) have been resolved from difference electron density.

Table 3. Crystallographic and Refinement Statistics

	Ac-AChBP + **31**	Ac-AChBP + **35**	Ac-AChBP Apo
	Crystallographic Statistics		
space group	$P3_121$	$C222_1$	$C222_1$
a, *b*, *c* (Å)	76.77, 76.77, 723.17	134.51, 173.63, 129.12	135.52, 175.94, 128.91
α, *β*, *γ* (deg)	90, 90, 120	90, 90, 90	90, 90, 90
resolution limits (Å)	44.6−2.7 (2.8−2.7)	106.0−2.60 (2.74−2.60)	52.06−1.90 (2.00−1.9)
R_{sym}	0.077 (0.491)	0.117 (0.547)	0.088 (0.603)
I/σ	9.9 (1.6)	5.6 (1.1)	5.5 (1.1)
multiplicity	8.8 (5.7)	2.5 (2.3)	3.4 (3.4)
completeness (%)	98.0 (98.0)	87.5 (52.8)	99.8 (100.0)
total number of reflections	594366 (33638)	101466 (8292)	405728 (59005)
number of unique reflections	67908 (5856)	40542 (3354)	121101 (17599)
	Refinement and Model Statistics		
R_{work} (%)	23.7	20.0	19.0
R_{free} (%)	26.7	25.0	23.1
rmsd bond distance (Å)	0.018	0.018	0.016
rmsd bond angle (deg)	1.591	1.65	1.583
average *B*-factors for AChBP, water, (ligand)	17, 46, 4	27, 31, 24	11, 18

obtained resolution of diffraction data (2.6−2.8 Å) we cannot exclude an alternative conformation in which the ethylene bridge of the tropine moiety faces the aromatic residues (parts D and F of Figure 5). However, this conformation may be less favorable because it partially shields the electron-rich cage formed by the aromatic residues from their cation−π interaction with the tropine nitrogen. Finally, comparison of the **31** and **35** complexes with Ac-AChBP (parts C and E of Figure 5) showed that the additional phenyl ring of **35**, which is attached to the tropine nitrogen, causes an outward movement of Tyr53 to accommodate the ligand within the binding pocket.

Docking of 31 and 35 in New Ac-AChBP Structures. The obtained crystal structures indicate an induced fit upon binding of **31** and **35**. To evaluate the in silico docking procedure, we have docked both compounds back into their respective crystal structures. The overall orientation of **31** was reproduced (rmsd

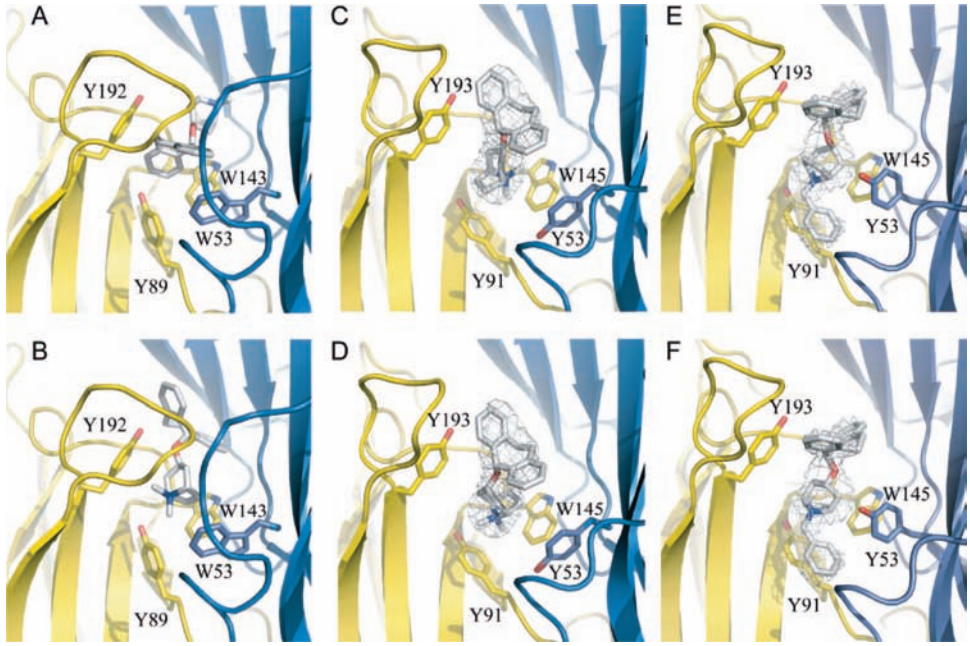

Figure 5. Using the in silico screen on Ls-AChBP, we identified two different binding poses for **31** (A and B). The cocrystal structures of Ac-AChBP with **31** (C and D) and **35** (E and F) clearly show a different binding pose in which the ligands have displaced loop C by ~5−6 Å. The most likely binding poses are depicted in parts C and E, since these orientations have more favorable cation−π interactions with Trp145.

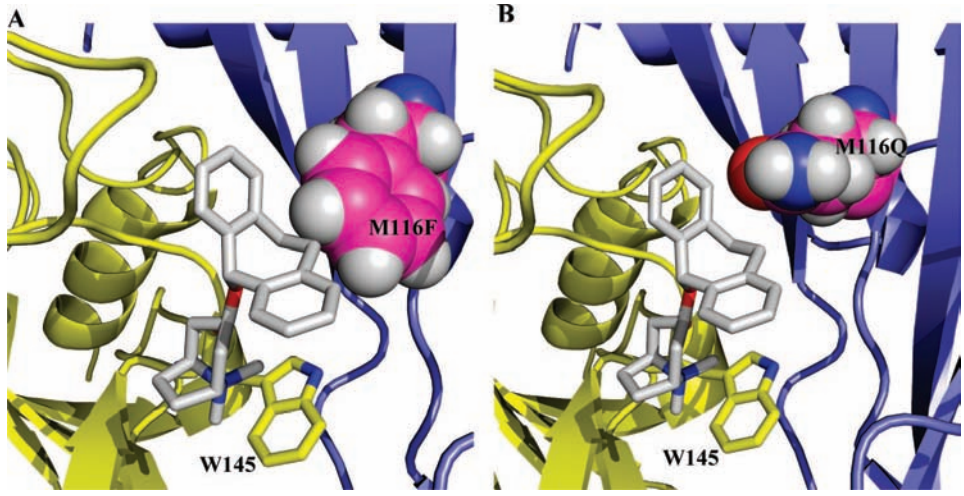

Figure 6. In silico mutations were made to understand the difference in binding affinity of the ligands for Ac-AChBP and the human nAChRs. (A) A M116F mutation (given in space-fill atom representation) was introduced in the Ac-AChBP cocrystal structure in complex with **31**, and a clear clash occurred between the aromatic residue and the tricyclic moiety of the ligand. (B) The same crystal structure was used to make the M116Q mutant (also in space-fill atom representation). No clash was observed, but the residue and the ligand could make contacts that are less favorable in the case of Gln compared to Met.

of 1.745−3.586 Å). This placed the ligand nitrogen in proximity to Trp145 and allowed for cation−π interactions to occur. However, the tricyclic moiety was docked in several distinct orientations with different dihedral angles around the ether bond. Compound **35** was positioned with the tropine moiety near Trp145, while the tricyclic group was within the aromatic cavity. This is a different pose than found in the crystal structure (rmsd of 7.431−7.877 Å).

In Silico Mutation of Ac-AChBP To Resemble Human α4β2 and α7 nAChRs. Simple in silico mutations were made using the obtained crystal structures to understand the difference in affinity of **31** and **35** for Ac-AChBP and both human nAChRs. Sequence analysis revealed that for human α4β2 and α7 nAChRs, Phe and Gln, respectively, are present at the Met116 position in Ac-AChBP. An in silico Met116Phe mutant was made in the cocrystal structure of **31** and Ac-AChBP. This indicated a clash between this aromatic residue and the tricyclic group of the ligands (Figure 6A). No clash was observed for the in silico Met116Gln mutant in the cocrystal structure of **31** and Ac-AChBP (Figure 6B).

Electrophysiology. Compounds **31** and **35** induce an intermediate open conformation of loop C. To evaluate the functional consequences of these conformational changes, we tested the effects of these two compounds on receptors expressed in *Xenopus* oocytes. Surprisingly, these ligands inhibited either the human α4β2 or α7 nAChRs with IC_{50} values in the micromolar range (parts A and B of Figure 7). Compounds **31** and **35** show comparable inhibition constants for both nAChRs with an IC_{50} value in the micromolar range, whereas these ligands lacked significant affinity in binding assays at the human α4β2 nAChR. Both compounds also inhibited the human $5HT_{3A}$ receptor with similar IC_{50} values (data not shown), suggesting a common

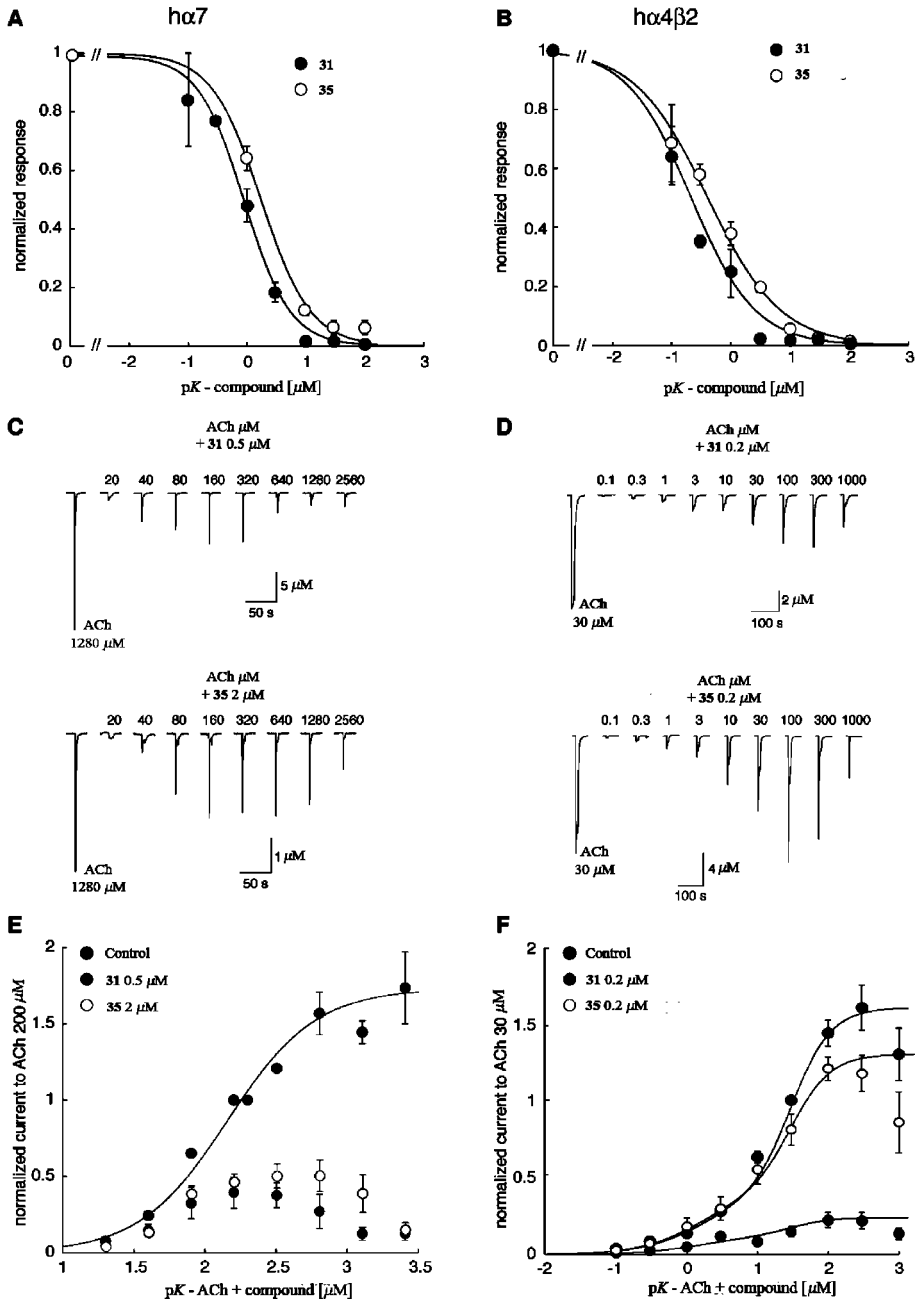

Figure 7. Effects of **31** and **35** on the functional properties of human α7 and α4β2 nAChRs. (A, B) Exposure to **31** and **35** inhibits, in a dose dependent manner, the acetylcholine-evoked currents. Data are readily fitted with a Hill equation and yielded IC_{50} values of 0.88 ± 0.1 and 1.73 ± 0.1 μM and nH of 1.1 ± 0.17 and 1.03 ± 0.05 for **31** ($n = 6$) and **35** ($n = 5$) at the human α7 receptor. IC_{50} values were 0.21 ± 0.1 and 0.46 ± 0.1 μM, and nH values were 0.9 ± 0.08 and 0.7 ± 0.03 for **31** ($n = 12$) and **35** ($n = 8$) at the human α4β2 receptor. (C−F) Determination of the concentration activation curves in the absence and presence of compounds **31** and **35**. Typical currents evoked by a series of acetylcholine concentration in the presence of **31** and **35** are shown for α7 and α4β2 in parts C and D. The first trace (1280 μM acetylcholine for α7 and 30 μM acetylcholine for α4β2) was recorded in control conditions and used for normalization. Plot of the peak current as a function of the logarithm of the acetylcholine concentration yielded typical concentration activation curves (E, F). Note that, given their inverted U shape, α7 responses could not be fitted by the empirical Hill equation. Good fits were obtained for α4β2 with a dual Hill equation with high affinity coefficients of EC_{50} of 1 μM and nH of 1 and low affinity coefficients of EC_{50} of 30 μM and nH of 1.5 and a fraction of high versus low affinity of 0.28. Curves obtained in the presence of 0.2 μM **31** and **35** were fitted with the same parameters using a scaling factor of 0.81 and 0.15, respectively ($n = 6$).

mechanism of blockade across this family of cationic ligand gated ion channels. To test this hypothesis further, acetylcholine concentration activation curves were measured at the α4β2 and α7 receptors in the absence or presence of 0.2 μM **31**, 0.2 μM **35** (Figure 7C−F). The lack of displacement of the acetylcholine sensitivity and the insurmountable inhibition both suggest that **31** and **35** are acting as noncompetitive inhibitors probably by entering the pore and steric hindrance.

The observation that both compounds inhibit α4β2 and α7 nAChRs in a noncompetitive manner came as a surprise because these compounds were initially tested in ^{125}I-Bgt displacement assays on human α7 nAChRs. In addition, they were cocrystallized at the binding pocket of Ac-AChBP, which is a structural homologue of the ligand-binding domain of nAChRs.

These findings were further investigated by performing radioligand saturation experiments to determine whether a

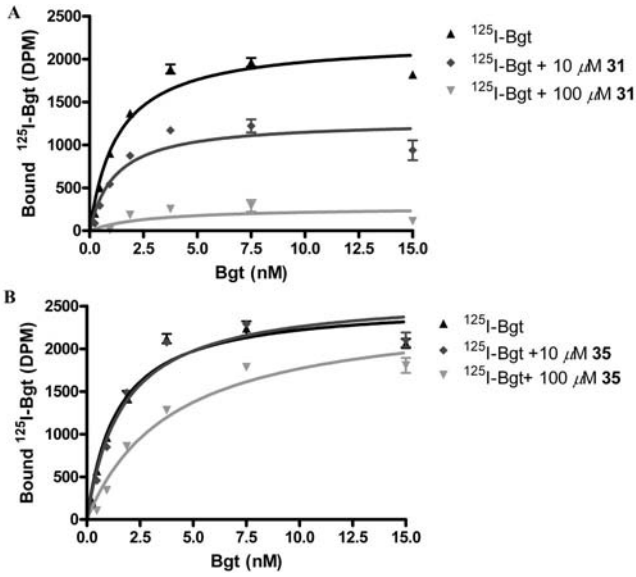

Figure 8. Radioligand saturation experiments on human α7 nAChR show that **31** (A) significantly diminishes the B_{max} value but leaves the K_d value unaffected. In contrast, 100 μM **35** (B) increases the K_d value and diminishes the B_{max}. No effect was observed on radioligand saturation for 10 μM **35**.

competitive component of ligand binding existed. A compound acting as a competitive inhibitor is expected to shift the K_d, whereas a noncompetitive inhibitor is expected to shift B_{max}. We observed that ^{125}I-Bgt saturation on the human α7 nAChR was affected by the presence of **31** and **35** but in a different way for each compound. Increasing amounts of **31** diminished B_{max} significantly, whereas little effect was observed for the K_d value of ^{125}I-Bgt (Figure 8A). This strongly suggests that **31** binds to an allosteric site, probably the ion channel pore. In contrast, ^{125}I-Bgt saturation curves in the presence of 100 μM **35** showed both a diminished B_{max} and an increased K_d value, indicative of both a noncompetitive and competitive component of antagonism (Figure 8B). This result suggests that **35** inhibits α7 nAChRs by dual binding to the extracellular ligand binding site and the ion channel pore.

^{3}H-epibatidine saturation curves for human α4β2 nAChRs were not affected by the presence of either **31** or **35**. Both the K_d and the B_{max} were unchanged, suggesting that inhibition of the α4β2 nAChR is caused purely by ion channel blockade. This was as expected, since both compounds did not show any affinity for α4β2 nAChR in displacement studies.

In view of the close structural homology between **31** or **35** and carbamazepine, we tested the action of this antiepileptic drug for ^{125}I-Bgt displacement on Ls-AChBP and human α7 nAChR and for [^{3}H]epibatidine displacement on human α4β2 nAChR. No radioligand displacement was observed for carbamazepine in all three displacement assays.

Discussion

In silico screening procedures are commonly used to identify novel hit compounds for protein targets of which structural information has been obtained. In this study, we applied a successful in silico screening of a proprietary compound collection containing druglike molecules against the crystal structures of Ls-AChBP. The in silico screening was performed on three available crystal structures of Ls-AChBP, i.e., in complex with carbamylcholine, HEPES, and nicotine. The protein structures obtained from the Ls-AChBP complexes with HEPES and nicotine were very useful, as these templates yielded high hit rates (81%); i.e., we selected 16 compounds for single point binding assays, and 13 compounds showed ^{125}I-Bgt displacement from Ls-AChBP at nicotine-like affinity. Compared to the much lower hit rate of a set of randomly selected compounds, the results indicate a significant enrichment of the in silico screen.

Interestingly, the carbamylcholine-bound Ls-AChBP structure failed to be a proper template for the in silico screening procedure. This structure has only a marginally lower resolution (2.5 Å) than the cocrystal structures of HEPES (2.1 Å) and nicotine (2.2 Å). It is noted that carbamylcholine could only be built in 3 of the 10 binding pockets of the two AChBP structures in the unit cell of the crystal structure. In comparison, nicotine could be built in all binding pockets and HEPES in three of the five binding pockets.[12] This low occupancy of carbamylcholine might indicate a lower probability of the observed binding pose. We have compared the AChBP protein structures in complex with carbamylcholine and nicotine. The rmsd measured over all atoms of the entire protein was 1.164 Å, and over all atoms of the binding-pocket (Ls-AChBP: W53, L102, R104, L112, M114, W143, Y185, C187, C188, and Y192) the rmsd value was 0.648 Å. Indeed, the superposition of the two structures revealed that the structural differences are small. However, it should be kept in mind that scoring functions are highly sensitive toward small conformational differences between protein structures. Our results show that ideally the use of several crystal structures should be considered for in silico screening efforts to improve the outcome.

In the past, AChBP has been cocrystallized with prototypical ligands that are known to bind to nAChRs. These include agonists (nicotine and epibatidine), partial agonists (lobeline), and antagonists such as cobratoxin and α-conotoxins. A consistent observation is that agonists stabilize loop C in a fully contracted state, whereas the peptide inhibitors stabilize loop C in a fully extended conformation. One exception is the nonpeptidic antagonist methyllycaconitine (MLA), which stabilizes loop C in an intermediate conformation.[8] Similarly, the ligands identified using our in silico screening stabilize loop C of AChBP in a conformation that is intermediate between the contracted and extended state observed in the crystal structures. This conformational state of AChBP is very similar to the "apo" structure of AChBP that was previously published by Hansen and colleagues.[8] However, it is important to note that an ordered PEG molecule could be built into electron density of the binding pocket, and therefore, this crystal structure probably does not reflect a true apo state. Recently, we have been able to crystallize Ac-AChBP in the absence of ligand or buffer molecules and demonstrated that the apo state of Ac-AChBP (parts A and B of Figure 4) is characterized by the presence of ordered water molecules in the binding pocket. This observation agrees well with results from molecular dynamics simulation of AChBP, suggesting that water molecules occupy the binding pocket at five distinct sites.[26] The cocrystal structures of AChBP with nicotine[12] and conotoxin ImI[7] have revealed that these water molecules can play an important role in forming hydrogen bonds between the ligand and residues of the binding site. More importantly, the apo state of Ac-AChBP is characterized by the lack of electron density at the tip of loop C despite the good resolution (1.9 Å) of the diffraction data (parts A and B of Figure 4). This indicates that this region of the protein is disordered in the crystal lattice and that this is most likely due to an intrinsic mobility of loop C. The movement of loop C is in line with several other experimental observations that loop C exerts fluctuating movements in the unliganded state of AChBPs and

nAChRs. For AChBP, the intrinsic flexibility of loop C has been demonstrated using tryptophan fluorescence[27] and molecular dynamics simulation.[26,27] Using hydrogen−deuterium exchange mass spectrometry,[28] Shi and colleagues demonstrated that loop C displays enhanced solvent exchange in the absence of ligand, suggesting that loop C exhibits rapid fluctuations in an open conformation. For nAChRs, targeted molecular dynamics simulation has demonstrated similar flexibility of loop C.[29]

We were interested in the functional characteristics of these compounds because they stabilize loop C in a conformation intermediate between the agonist- and antagonist-bound state of AChBP. Additionally, **35** causes an outward rotation of Tyr53 in the binding pocket, a residue that has recently been implicated in the desensitization of the α7 nAChR.[30] Although distinct conformational states seem to be stabilized by the two compounds, our current knowledge of the receptor is insufficient to predict the functional outcomes of such differences. To address this issue further, we therefore examined the effects of **31** and **35** at receptors expressed in *Xenopus* oocytes. The unexpected observation that both compounds significantly inhibit the α4β2 and α7 receptors suggested that additional mechanisms of ligand−receptor interaction could be present. As both **31** and **35** showed an insurmountable inhibition of acetylcholine-evoked responses of the α4β2 nAChR, we concluded that these compounds functionally act as noncompetitive inhibitors. Moreover, the magnitude of blockade probably occludes the plausible interaction that these compounds can have at the acetylcholine binding site. This hypothesis is confirmed by the fact that both compounds were found to inhibit in a similar manner the closely related cationic ligand gated channel $5HT_3R$.

Interestingly, while this work was being finalized, Gumilar and Bouzat[31] reported that well-known tricyclic antidepressants, i.e., imipramine (Figure 2), amitriptyline, and doxepin, inhibit Cys-loop receptors by acting through different mechanisms at open and closed conformational states. Patch-clamp recording studies using high conductance forms of α7-$5HT_{3A}$ chimeric receptors and high conductant $5HT_{3A}$ receptors suggested that the tricyclic compounds have more than one site of action, namely, at the ion pore in the open state and at the extracellular domain in the closed state. The crystal structures presented here strongly support these recent insights and suggest that this extracellular site is actually the orthosteric binding site. The series of close analogues might be ideal molecular tools to probe the different binding sites in these advanced electrophysiological experiments.

The obtained cocrystal structures allow us to speculate on the lack of affinity of **31** and **35** for the human α4β2 nAChR. Probably, the lack of affinity of both compounds for α4β2 nAChR is caused by Phe144 (counterpart Met116 Ac-AChBP), which clashes with the tricyclic moiety of the ligands. A Gln residue in the same position of the α7 nAChR binding pocket does not hinder binding of these ligands.

The crystal structures have provided us with important clues for structure-based hit-optimization procedures. These structures clearly indicate that there is a cation−π interaction present between Trp145 and the tropine moiety of the ligands. We expect that the tropine moiety of the ligands is crucial in binding to both AChBPs and nAChRs. In addition, Tables 1 and 2 show that the tropine containing ligands have significantly higher affinities than their piperidine containing analogues. The tropine functionality is also found in the α7 partial agonist tropisetron.[32] The structures also show that there is significant conformational freedom in the orientation of the tricyclic moiety. Hydrophobic interactions between the dibenzosuberyl moiety and the binding pocket are present, but there are no hydrogen bonds or electrostatic interactions that force directionality upon the tricyclic group. This finding is also illustrated by the docking of **31** and **35** into their crystal structures.

The bulky tricyclic moiety forces loop C to move away from the binding pocket by steric clashes and might therefore rule out agonism, which is assumed to require a fully contracted conformation of loop C.

Conclusion

In summary, we have shown that AChBP is a good structural template for the identification of nAChR ligands in an in silico screening procedure. The HEPES and nicotine bound structures performed better than the carbamylcholine bound structure and were able to identify ligands with similar affinity as nicotine. This clearly shows that the use of several crystal structures should be considered to improve the hit-rate of the in silico screening. A subsequent similarity search of hit-compounds in our proprietary database was performed, and compounds with nicotine-like affinity and α7 nAChR selectivity were obtained. Two of these compounds were subsequently cocrystallized in Ac-AChBP. These complexes have provided interesting insights and new possibilities for future structure-based hit-optimization procedures to obtain selective nAChR ligands. Differences observed between ligand binding and functional assays highlight the need for combined experiments and further knowledge of the three-dimensional structure of the receptor.

Materials and Methods

Proprietary Compound Collection. A proprietary compound library containing more than 5000 structurally diverse and druglike compounds was used in our in silico screening procedure. This database was obtained from a discontinued pharmaceutical company (personal gift of H. Timmerman) and was mainly targeting G-protein-coupled receptors (GPCRs) involved in inflammation, allergy, and pain. This database also contained antidepressants and neuroleptics. This database was not developed specifically against ligand-gated ion channels, and it was not likely that the majority of the compounds had any affinity for our target protein.

Database Preparation. The compound collection was stored in digital format, and three-dimensional structures were generated using MOE (version 2004.03, Chemical Computing Group, Montreal, Canada). Counterions and solvents were filtered out, and protonation was set such that all acids and bases were charged. Partial atomic charges were calculated, and the molecules were energy-minimized in vacuo using the MMFF94x force field in MOE.

Template Preparation. Three available Ls-AChBP crystal structures were used in the docking procedure, namely, Ls-AChBP in complex with carbamylcholine (PDB accession code 1uv6, 2.5 Å), HEPES (PDB accession code 1ux2, 2.1 Å), and nicotine (PDB accession code 1uw6, 2.2 Å). The ligand and water molecules were removed, and hydrogen atoms were added to the protein models. Partial atomic charges were calculated, and energy minimization was performed using the AMBER99 force field in MOE. The docking procedure was performed in only one binding pocket formed by adjacent subunits.

In Silico Screening Procedure. Docking studies were performed using the GOLD docking program (version 2.0)[21] and the GoldScore scoring function and default settings. For each ligand the binding pose with the highest score was determined, and all ligands were ranked according to their scores. The top-ranked 50 compounds were visually inspected to verify optimal binding in terms of hydrogen bonding directionality and steric complementarity of ligand and receptor. A diverse and high-ranked subset of ligands was selected for binding assays.

Expression and Purification of AChBPs and nAChRs. Ac-AChBP and Ls-AChBP were expressed from baculovirus using the

pFastbac I vector in Sf9 insect cells and purified from medium as described.[12] Human neuroblastoma cells (SH-SY5Y) expressing human α7 nAChRs were obtained from Christian Fuhrer (Department of Neurochemistry, Brain Research Institute, University of Zurich).[25]

Human α4*β*2 nAChRs were obtained using a transient transfection of HEK293t cells. To this end, HEK293t cells were maintained in Dulbecco's modified Eagle medium (DMEM) supplemented with 10% fetal calf serum (FCS), 50 IU/mL penicillin, and 50 μg/mL streptomycin in 5% CO_2 humidified atmosphere at 37 °C. Approximately 2 million cells were seeded in a 10 cm dish and cultured overnight before transfection. For transfection of each dish of cells, the transfection mixture was prepared in 0.6 mL of PBS and contained 0.3 μg of human α4 subunit plasmid, 2.7 μg of human *β*2 subunit plasmid, 3.0 μg of ric3, and 24 μL of 1 mg/mL 25 kDa linear polyethyleneimine (Polyscience, Inc.). The mixture was incubated for 10−15 min at room temperature before it was added into the monolayer cell culture loaded with 6 mL of fresh and prewarmed cell culture medium. Two days after transfection, the cells were washed with PBS, collected as pellet by centrifuging, and stored at −80 °C until use.

Radioligand Binding Assay on AChBPs. Competition binding assays were performed with His-tagged Ls-AChBP or Ac-AChBP in buffer (PBS, 20 mM Tris, 1 mg/mL BSA, pH 8.0) in a final assay volume of 100 μL. A constant concentration of [^{125}I]α-bungarotoxin (^{125}I-Bgt, GE Healthcare, specific activity of ∼182 Ci/mmol, 1 nM) or [^{3}H]epibatidine (GE Healthcare, specific activity of ∼2 Ci/mmol, 3 nM) was used for Ls-AChBP or Ac-AChBP, respectively. The concentrations of radioligand were chosen at the K_d value for the target protein. The amounts of protein, ^{125}I-Bgt, and [^{3}H]epibatidine were chosen as such that we obtained a clear window in the displacement curve, sufficient amount of counts in our scintillation counting, and a radioligand depletion of less than 10%. Ligands were added together with TALON metal affinity resins (Clontech), which were prewashed with assay buffer and incubated for 1.5 h at room temperature under continuous shaking. Bound radioligand was collected on 0.3% polyethyleneimine-pretreated Unifilter-96 GF/C filters (Perkin-Elmer) using ice-cold 50 mM Tris buffer at pH 7.5. After the filters were dried, scintillation fluid (MicroScint, Perkin-Elmer) was added and the radioactivity was measured in a Wallac 1450 MicroBeta liquid scintillation counter.

In our single point assay on Ls-AChBP, ^{125}I-Bgt displacement was measured in the presence of 100 μM ligand and the results were compared to ^{125}I-Bgt displacement in the presence of 50 μM nicotine. The total ^{125}I-Bgt binding in the absence of ligands was set at 100%.

Radioligand Binding Assay on nAChRs. Binding assays for human α4*β*2 and α7 nAChRs were performed in a similar way as described for Ls-AChBP; however, no TALON metal affinity resins were added. The cells were homogenized immediately before use. In the α4*β*2 assay, [^{3}H]epibatidine was used at a final concentration of 100 pM, and for the α7 assay ^{125}I-Bgt was used at a concentration of 2 nM.

Radioligand saturation experiments were performed with nicotine to determine nonspecific binding. The concentration of nicotine was 100 μM for the α4*β*2 nAChR and 1 mM for the α7 nAChR.

Data Analysis. All radioligand binding data were evaluated by a nonlinear, least-squares curve fitting procedure using Graphpad Prism (version 4.01, GraphPad Software, Inc., San Diego, CA). All data are represented as the mean ± SEM from at least three independent experiments.

Electrophysiology. Expression and electrophysiological recordings from nAChRs were carried out as described previously.[33] Briefly, oocytes were injected intranuclearly with 2 ng of cDNA that encoded the human α4*β*2, α7 nAChR or $5HT_{3A}$ receptors. All recordings were performed in OR2 medium that contained 82.5 mM NaCl, 2.5 mM KCl, 5 mM $CaCl_2$, and 2 mM HEPES (pH 7.4) adjusted with NaOH. Acetylcholine, **31**, and **35** were dissolved in the solution just before use. To prevent contamination by the activation of calcium-dependent chloride channels, oocytes were incubated for at least 3 h in the presence of the chelating agent 1,2-bis(2-aminophenoxy)ethane-*N*,*N*,*N*′,*N*′-tetraacetate-acetoxymethyl ester (100 μM). Unless indicated, all recordings were performed at −100 mV; data were digitized online and analyzed off-line using MATLAB (Mathworks, Natick, MA). Concentration−inhibition curves were fitted with a single equation in the form

$$y = \frac{1}{1 + \frac{x}{IC_{50}}}$$

where y is the amplitude of current normalized versus the maximal response, x is the concentration of antagonist, and IC_{50} the half-inhibition. Concentration−activation curves were fitted with a single Hill equation for α7 and a dual Hill equation for α4*β*2 in the form

$$y = I_{max}\left(\frac{a}{1 + (EC_{50}H/x)^{nH1}}\right) + \frac{1 - a}{1 + (EC_{50}L/x)^{nH2}}$$

I_{max} is the maximal current amplitude normalized versus the amplitude of the reference test pulse, and x is the agonist concentration. $EC_{50}H$, nH1, and a are respectively the half-effective concentration, the Hill coefficient, and the percentage of receptors in the high-affinity state, whereas $EC_{50}L$ and nH2 correspond to the half-effective concentration and the Hill coefficient in the low-affinity state.

Compound Synthesis and Validation. To validate the chemical structures of **31** and **35**, a resynthesis was performed using a slightly modified procedure described by van der Stelt et al.[34,35] Toluene was used instead of benzene in the synthesis of 5-chloro-10,11-dihydro-5*H*-dibenzo[7]annulene (quantitative yield). In the preparation of dibenzheptropine, xylene was replaced for toluene and the reaction was performed at room temperature instead of under reflux conditions (63% isolated yield). Benzylation of dibenzhepnortropine was not performed with benzyl bromide but via a reductive amination procedure (60% isolated yield) as described by Abdel-Magid et al.[36] Analytical characterization confirmed the chemical structures. Compound **31**: mp 192.7−194.0 °C (lit. mp 190−191);[34] ^{1}H NMR (CD_3OD, 200 MHz) δ 7.36 (d, 2H), 6.90−7.28 (m, 6H), 5.39 (br s, 1H), 3.80 (br s, 2H), 3.68 (br s, 2H), 3.09 (d, 6H), 2.95 (br s, 2H), 1.97−2.55 (m, 8H); ^{13}C NMR (CD_3OD, 50 MHz) δ 131.5, 129.5, 127.1, 69.5, 51.5, 44.7, 33.4, 32.9, 26.2; LC/MS purity (λ = 254 nm) >99%, *m*/*z* 348.2 (M^+). Compound **35**: mp 174.5−175.5 (lit. mp 175−178);[35] ^{1}H NMR ($CDCl_3$, 200 MHz) δ 11.80 (br s, 1H), 7.38 (s, 5H), 6.92−7.30 (m, 8H), 6.76 (s, 2H), 5.10 (br s, 1H), 4.09 (s, 2H), 3.71 (s, 2H), 3.58 (br s, 2H), 2.94 (br s, 2H), 1.90−2.62 (m, 8H); ^{13}C NMR ($CDCl_3$, 50 MHz) δ 169.3, 135.6, 130.4, 130.2, 129.8, 129.3, 129.2, 125.9, 67.3, 59.5, 54.4, 34.2, 32.0, 24.6; LC/MS purity (λ = 254 nm) >99%, *m*/*z* 410.3 (M + H).

Crystallography. Crystal screens for Ac-AChBP in complex with **31** and **35** were set up using nanoliter crystallization robotics[37] (TTP LabTech, Hertfordshire, U.K.). Crystals for Ac-AChBP in complex with **31** were obtained with 100−150 mM $CaCl_2$, 22−26% PEG400, and 100 mM HEPES at pH 7.5 in the crystallization buffer. For Ac-AChBP in complex with **35** crystallization conditions were 2 M Na formate and 0.1 M NaOAc at pH 4.5. For apo Ac-AChBP, crystallization conditions were 50 mM LiCl, 11−13% PEG6000, and 100 mM MES at pH 6.0. The "apo" crystals were grown in the presence of 300 μM ImII[38] in an attempt to cocrystallize Ac-AChBP with ImII. However, this peptide binds with low affinity to Ac-AChBP (data not shown) and could not be localized in the electron density map. The conformational state is therefore referred to as "apo". Cryoprotection was achieved by adding PEG400 to the mother liquor for **31** cocrystals and glycerol for apo and **35** cocrystals. Crystals were flash-frozen by immersion in liquid nitrogen. Diffraction data for Ac-AChBP in complex with **31** were collected at beamline BM-14 at the European Synchrotron Radiation Facility, Grenoble, France. Data were indexed and processed with DENZO and SCALEPACK, and a first data set with

acceptable merging statistics was obtained to 3.3 Å resolution. The crystal belongs to space group $P3_121$ and has the following cell dimensions: $a = 76.81$ Å, $b = 76.81$ Å, $c = 725.52$ Å, $\alpha = 90.0°$, $\beta = 90.0°$, $\gamma = 120.0°$. The structure was solved by molecular replacement using MOLREP and the open C-loop structure of Ac-AChBP as the search model (PDB accession code 2c9t). The initial model was refined with REFMAC[39] using NCS and TLS[40] restraints. A second data set with diffraction data beyond 2.8 Å resolution was collected at beamline X06SA at the Swiss Light Source, Villigen Switzerland. Several technical measures were required to minimize spot overlaps along the 725 Å axis, including alignment of the crystal with the long cell axis along the rotation axis, reduction of the beam size, and focusing of the beam onto the detector. Data were processed with EVAL15[41] to correct for residual spot overlaps. The model was further refined with REFMAC to $R_{work} = 23.7\%$ and $R_{free} = 26.7\%$.

Diffraction data for Ac-AChBP in complex with **35** were obtained at beamline EH14-4 of the European Synchrotron Radiation Facility, Grenoble, France. Diffraction data were indexed and integrated with MOSFLM; scaling was done with SCALA.[39] The crystal belongs to space group $C222_1$ and has the following cell dimensions: $a = 134.07$ Å, $b = 173.45$ Å, $c = 128.99$ Å, $\alpha = 90.0°$, $\beta = 90.0°$, $\gamma = 90.0°$. The structure was solved by molecular replacement with PHASER[42] using the open C-loop structure as the search model (PDB accession code 2c9t). **31** and **35** were automatically fit into difference electron density in some binding sites by the automatic ligand-fitting procedure in COOT.[43] The complexes were refined with additional restraints for **31** or **35** obtained from the PRODRG server.[44]

Diffraction data for Ac-AChBP in the apo state were obtained at beamline EH14-1 of the European Synchrotron Radiation Facility, Grenoble, France. Diffraction data were indexed and integrated with MOSFLM; scaling was done with SCALA.[39] The crystal belongs to space group $C222_1$ and has the following cell dimensions: $a = 135.87$ Å, $b = 176.26$ Å, $c = 129.05$ Å, $\alpha = 90.0°$, $\beta = 90.0°$, $\gamma = 90.0°$. The structure was solved by molecular replacement using MOLREP and the open C-loop structure of Ac-AChBP as the search model (PDB accession code 2c9t). The initial model was refined with REFMAC[39] and automatically rebuilt with flex-wARP.[45]

Manual structure building was carried out with COOT.[43] Structure validation was done with WHATIF[46] and MOLPROBITY.[47] Figures were prepared with PYMOL (DeLano Scientific, San Carlos, CA).

Acknowledgment. We thank beamline staff at European Synchrotron Radiation Facility, Grenoble, France, and Swiss Light Source, Villigen, Switzerland, for assistance with data collection, and we thank members of the Sixma and Perrakis laboratory for comments and suggestions with regard to solving the crystal structure. Toine Schreurs and Loes Kroon-Batenburg are acknowledged for processing data with EVAL, Judith Smit and Igor Kasheverov for assistance with crystallization screens, and Ewald Edink for synthesis. This work was supported by a Netherlands Technology Foundation Grant BBC6035 (to T.K.S. and A.B.S.), a long-term fellowship from the European Molecular Biology Organization (to C.U.), a personal mozaiek grant from The Netherlands Organization for Scientific Research (NWO) (to A.A.), the Swiss National Science Foundation (to D.B.), and the EEC grant (NeuroCypress).

References

(1) Jensen, A. A.; Frolund, B.; Liljefors, T.; Krogsgaard-Larsen, P. Neuronal nicotinic acetylcholine receptors: structural revelations, target identifications, and therapeutic inspirations. *J. Med. Chem.* **2005**, *48*, 4705–4745.

(2) de Jonge, W. J.; Ulloa, L. The alpha7 nicotinic acetylcholine receptor as a pharmacological target for inflammation. *Br. J. Pharmacol.* **2007**, *151*, 915–929.

(3) Mudo, G.; Belluardo, N.; Fuxe, K. Nicotinic receptor agonists as neuroprotective/neurotrophic drugs. Progress in molecular mechanisms. *J. Neural Transm.* **2007**, *114*, 135–147.

(4) Keating, G. M.; Siddiqui, M. A. Varenicline: a review of its use as an aid to smoking cessation therapy. *CNS Drugs* **2006**, *20*, 945–960.

(5) Smit, A. B.; Syed, N. I.; Schaap, D.; van Minnen, J.; Klumperman, J.; Kits, K. S.; Lodder, H.; van der Schors, R. C.; van Elk, R.; Sorgedrager, B.; Brejc, K.; Sixma, T. K.; Geraerts, W. P. A glia-derived acetylcholine-binding protein that modulates synaptic transmission. *Nature (London)* **2001**, *411*, 261–268.

(6) Brejc, K.; van Dijk, W. J.; Klaassen, R. V.; Schuurmans, M.; van Der Oost, J.; Smit, A. B.; Sixma, T. K. Crystal structure of an ACh-binding protein reveals the ligand-binding domain of nicotinic receptors. *Nature (London)* **2001**, *411*, 269–276.

(7) Ulens, C.; Hogg, R. C.; Celie, P. H.; Bertrand, D.; Tsetlin, V.; Smit, A. B.; Sixma, T. K. Structural determinants of selective alpha-conotoxin binding to a nicotinic acetylcholine receptor homolog AChBP. *Proc. Natl. Acad. Sci. U.S.A.* **2006**, *103*, 3615–3620.

(8) Hansen, S. B.; Sulzenbacher, G.; Huxford, T.; Marchot, P.; Taylor, P.; Bourne, Y. Structures of Aplysia AChBP complexes with nicotinic agonists and antagonists reveal distinctive binding interfaces and conformations. *EMBO J.* **2005**, *24*, 3635–3646.

(9) Hansen, S. B.; Talley, T. T.; Radic, Z.; Taylor, P. Structural and ligand recognition characteristics of an acetylcholine-binding protein from *Aplysia californica*. *J. Biol. Chem.* **2004**, *279*, 24197–24202.

(10) Celie, P. H.; Klaassen, R. V.; van Rossum-Fikkert, S. E.; van Elk, R.; van Nierop, P.; Smit, A. B.; Sixma, T. K. Crystal structure of acetylcholine-binding protein from *Bulinus truncatus* reveals the conserved structural scaffold and sites of variation in nicotinic acetylcholine receptors. *J. Biol. Chem.* **2005**, *280*, 26457–26466.

(11) Celie, P. H.; Kasheverov, I. E.; Mordvintsev, D. Y.; Hogg, R. C.; van Nierop, P.; van Elk, R.; van Rossum-Fikkert, S. E.; Zhmak, M. N.; Bertrand, D.; Tsetlin, V.; Sixma, T. K.; Smit, A. B. Crystal structure of nicotinic acetylcholine receptor homolog AChBP in complex with an alpha-conotoxin PnIA variant. *Nat. Struct. Mol. Biol.* **2005**, *12*, 582–588.

(12) Celie, P. H.; van Rossum-Fikkert, S. E.; van Dijk, W. J.; Brejc, K.; Smit, A. B.; Sixma, T. K. Nicotine and carbamylcholine binding to nicotinic acetylcholine receptors as studied in AChBP crystal structures. *Neuron* **2004**, *41*, 907–914.

(13) Dutertre, S.; Ulens, C.; Buttner, R.; Fish, A.; van Elk, R.; Kendel, Y.; Hopping, G.; Alewood, P. F.; Schroeder, C.; Nicke, A.; Smit, A. B.; Sixma, T. K.; Lewis, R. J. AChBP-targeted alpha-conotoxin correlates distinct binding orientations with nAChR subtype selectivity. *EMBO J.* **2007**, *26*, 3858–3867.

(14) Hilf, R. J.; Dutzler, R. X-ray structure of a prokaryotic pentameric ligand-gated ion channel. *Nature (London)* **2008**, *452*, 375–379.

(15) Lyne, P. D. Structure-based virtual screening: an overview. *Drug Discovery Today* **2002**, *7*, 1047–1055.

(16) Alvarez, J. C. High-throughput docking as a source of novel drug leads. *Curr. Opin. Chem. Biol.* **2004**, *8*, 365–370.

(17) Zhao, L.; Brinton, R. D. Structure-based virtual screening for plant-based ERbeta-selective ligands as potential preventative therapy against age-related neurodegenerative diseases. *J. Med. Chem.* **2005**, *48*, 3463–3466.

(18) Lu, I. L.; Huang, C. F.; Peng, Y. H.; Lin, Y. T.; Hsieh, H. P.; Chen, C. T.; Lien, T. W.; Lee, H. J.; Mahindroo, N.; Prakash, E.; Yueh, A.; Chen, H. Y.; Goparaju, C. M.; Chen, X.; Liao, C. C.; Chao, Y. S.; Hsu, J. T.; Wu, S. Y. Structure-based drug design of a novel family of PPARgamma partial agonists: virtual screening, X-ray crystallography, and in vitro/in vivo biological activities. *J. Med. Chem.* **2006**, *49*, 2703–2712.

(19) Abagyan, R.; Totrov, M. High-throughput docking for lead generation. *Curr. Opin. Chem. Biol.* **2001**, *5*, 375–382.

(20) Taylor, R. D.; Jewsbury, P. J.; Essex, J. W. A review of protein-small molecule docking methods. *J. Comput.-Aided Mol. Des.* **2002**, *16*, 151–166.

(21) Jones, G.; Willett, P.; Glen, R. C.; Leach, A. R.; Taylor, R. Development and validation of a genetic algorithm for flexible docking. *J. Mol. Biol.* **1997**, *267*, 727–748.

(22) Arita, M.; Wada, A.; Takara, H.; Izumi, F. Inhibition of ^{22}Na influx by tricyclic and tetracyclic antidepressants and binding of [^{3}H]imipramine in bovine adrenal medullary cells. *J. Pharmacol. Exp. Ther.* **1987**, *243*, 342–348.

(23) Briggs, C. A.; Schrimpf, M. R.; Anderson, D. J.; Gubbins, E. J.; Gronlien, J. H.; Hakerud, M.; Ween, H.; Thorin-Hagene, K.; Malysz, J.; Li, J.; Bunnelle, W. H.; Gopalakrishnan, M.; Meyer, M. D. alpha7 nicotinic acetylcholine receptor agonist properties of tilorone and related tricyclic analogues. *Br. J. Pharmacol.* **2008**, *153*, 1054–1061.

(24) Peng, X.; Katz, M.; Gerzanich, V.; Anand, R.; Lindstrom, J. Human alpha 7 acetylcholine receptor: cloning of the alpha 7 subunit from the SH-SY5Y cell line and determination of pharmacological properties of native receptors and functional alpha 7 homomers expressed in Xenopus oocytes. *Mol. Pharmacol.* **1994**, *45*, 546–554.

(25) Charpantier, E.; Wiesner, A.; Huh, K. H.; Ogier, R.; Hoda, J. C.; Allaman, G.; Raggenbass, M.; Feuerbach, D.; Bertrand, D.; Fuhrer, C. Alpha7 neuronal nicotinic acetylcholine receptors are negatively regulated by tyrosine phosphorylation and Src-family kinases. *J. Neurosci.* **2005**, *25*, 9836–9849.
(26) Amiri, S.; Sansom, M. S.; Biggin, P. C. Molecular dynamics studies of AChBP with nicotine and carbamylcholine: the role of water in the binding pocket. *Protein Eng. Des. Sel.* **2007**, *20*, 353–359.
(27) Gao, F.; Bren, N.; Burghardt, T. P.; Hansen, S.; Henchman, R. H.; Taylor, P.; McCammon, J. A.; Sine, S. M. Agonist-mediated conformational changes in acetylcholine-binding protein revealed by simulation and intrinsic tryptophan fluorescence. *J. Biol. Chem.* **2005**, *280*, 8443–8451.
(28) Shi, J.; Koeppe, J. R.; Komives, E. A.; Taylor, P. Ligand-induced conformational changes in the acetylcholine-binding protein analyzed by hydrogen-deuterium exchange mass spectrometry. *J. Biol. Chem.* **2006**, *281*, 12170–12177.
(29) Cheng, X.; Wang, H.; Grant, B.; Sine, S. M.; McCammon, J. A. Targeted molecular dynamics study of C-loop closure and channel gating in nicotinic receptors. *PLoS Comput. Biol.* **2006**, *2*, e134.
(30) Gay, E. A.; Giniatullin, R.; Skorinkin, A.; Yakel, J. L. Aromatic residues at position 55 of rat alpha7 nicotinic acetylcholine receptors are critical for maintaining rapid desensitization. *J. Physiol.* **2008**, *586*, 1105–1115.
(31) Gumilar, F.; Bouzat, C. Tricyclic antidepressants inhibit homomeric Cys-loop receptors by acting at different conformational states. *Eur. J. Pharmacol.* **2008**, *584*, 30–39.
(32) Macor, J. E.; Gurley, D.; Lanthorn, T.; Loch, J.; Mack, R. A.; Mullen, G.; Tran, O.; Wright, N.; Gordon, J. C. The 5-HT3 antagonist tropisetron (ICS 205-930) is a potent and selective alpha7 nicotinic receptor partial agonist. *Bioorg. Med. Chem. Lett.* **2001**, *11*, 319–321.
(33) Hogg, R. C.; Hopping, G.; Alewood, P. F.; Adams, D. J.; Bertrand, D. Alpha-conotoxins PnIA and [A10L]PnIA stabilize different states of the alpha7-L247T nicotinic acetylcholine receptor. *J. Biol. Chem.* **2003**, *278*, 26908–26914.
(34) van der Stelt, C.; Harms, A. F.; Nauta, W. T. The effect of alkylsubstitution in drugs. V. Synthesis and chemical properties of some dibenzo[*a*,*d*]1,4-cycloheptadienyl ethers. *J. Med. Pharm. Chem.* **1961**, *4*, 335–49.
(35) van der Stelt, C.; Funcke, A. B.; Tersteege, H. M.; Nauta, W. T. The effect of alkyl substitution in drugs. XVI. Basic ethers of 10,11-dihydro-5H-dibenzo[*a*,*d*]cyclohepten-5-ol and some related compounds. *Arzneim.-Forsch.* **1966**, *16*, 1342–1345.
(36) Abdel-Magid, A. F.; Carson, K. G.; Harris, B. D.; Maryanoff, C. A.; Shah, R. D. Reductive amination of aldehydes and ketones with sodium triacetoxyborohydride. Studies on direct and indirect reductive amination procedures. *J. Org. Chem.* **1996**, *61*, 3849–3862.
(37) Newman, J.; Egan, D.; Walter, T. S.; Meged, R.; Berry, I.; Ben Jelloul, M.; Sussman, J. L.; Stuart, D. I.; Perrakis, A. Towards rationalization of crystallization screening for small- to medium-sized academic laboratories: the PACT/JCSG+ strategy. *Acta Crystallogr., Sect. D: Biol. Crystallogr.* **2005**, *61*, 1426–1431.
(38) Ellison, M.; Gao, F.; Wang, H. L.; Sine, S. M.; McIntosh, J. M.; Olivera, B. M. Alpha-conotoxins ImI and ImII target distinct regions of the human alpha7 nicotinic acetylcholine receptor and distinguish human nicotinic receptor subtypes. *Biochemistry* **2004**, *43*, 16019–16026.
(39) The CCP4 suite: programs for protein crystallography. *Acta Crystallogr., Sect. D: Biol. Crystallogr.* **1994**, *50*, 760−763.
(40) Winn, M. D.; Isupov, M. N.; Murshudov, G. N. Use of TLS parameters to model anisotropic displacements in macromolecular refinement. *Acta Crystallogr., Sect. D: Biol. Crystallogr.* **2001**, *57*, 122–133.
(41) Duisenberg, A. J. M.; Kroon-Batenburg, L. M. J.; Schreurs, A. M. M. An intensity evaluation method: EVAL-14. *J. Appl. Crystallogr.* **2003**, 220–229.
(42) McCoy, A. J.; Grosse-Kunstleve, R. W.; Storoni, L. C.; Read, R. J. Likelihood-enhanced fast translation functions. *Acta Crystallogr., Sect. D: Biol. Crystallogr.* **2005**, *61*, 458–464.
(43) Emsley, P.; Cowtan, K. Coot: model-building tools for molecular graphics. *Acta Crystallogr., Sect. D: Biol. Crystallogr.* **2004**, *60*, 2126–2132.
(44) Schuttelkopf, A. W.; van Aalten, D. M. PRODRG: a tool for high-throughput crystallography of protein−ligand complexes. *Acta Crystallogr., Sect. D: Biol. Crystallogr.* **2004**, *60*, 1355–1363.
(45) Cohen, S. X.; Morris, R. J.; Fernandez, F. J.; Ben Jelloul, M.; Kakaris, M.; Parthasarathy, V.; Lamzin, V. S.; Kleywegt, G. J.; Perrakis, A. Towards complete validated models in the next generation of ARP/wARP. *Acta Crystallogr., Sect. D: Biol. Crystallogr.* **2004**, *60*, 2222–2229.
(46) Hooft, R. W.; Vriend, G.; Sander, C.; Abola, E. E. Errors in protein structures. *Nature (London)* **1996**, *381*, 272.
(47) Davis, I. W.; Murray, L. W.; Richardson, J. S.; Richardson, D. C. MOLPROBITY: structure validation and all-atom contact analysis for nucleic acids and their complexes. *Nucleic Acids Res.* **2004**, *32*, W615–W619.

JM801400G